Journal of Applied Polymer Science

Preparation and Study of Intumescent Flame Retardant Poly(butylene succinate) Using MgAlZnFe-CO_3 Layered Double Hydroxide as a Synergistic Agent

Yue-Jun Liu, Long Mao, Shu-hong Fan
Key Laboratory of New Materials and Technology for Packaging, College of Packaging and Materials Engineering, Hunan University of Technology, Zhuzhou 412007, China
Correspondence to: Y.-J. Liu (E-mail: yjliu_2005@126.com)

ABSTRACT: Intumescent flame retardant consisting of ammonium polyphosphate and melamine, and MgAlZnFe-CO_3 layered double hydroxides (LDHs) prepared by the constant pH coprecipitation method, were added to poly(butylene succinate) (PBS) via melt blending to obtain novel intumescent flame retardant poly(butylene succinate) (IFR-PBS) composites. A study on the effect of MgAlZnFe-CO_3 LDHs on the mechanical, thermal, and flame retardancy properties of IFR-PBS composites was investigated. It was revealed that IFR-PBS composites exhibited both excellent flame retardancy and antidripping properties when the content of MgAlZnFe-CO_3 LDHs was 1% (the total loading of flame retardant was 20%), for a goal of vertical flammability (UL-94) V-0 rate and a limiting oxygen index value of 35. The results showed that a suitable amount of MgAlZnFe-CO_3 LDHs had a noticeable synergistic effect on IFR-PBS composites. Importantly, tensile strength and flexural strength were improved by the presence of MgAlZnFe-CO_3 LDHs. © 2014 Wiley Periodicals, Inc. J. Appl. Polym. Sci. **2014**, *131*, 40736.

KEYWORDS: biodegradable; composites; flame retardance

Received 6 October 2013; accepted 20 March 2014
DOI: 10.1002/app.40736

INTRODUCTION

In recent years, aliphatic polyesters have attracted great interest due to their outstanding biodegradability and biocompatibility. As one of the most promising candidates in the field of bio-based plastics for its biodegradability, poly(butylene succinate) (PBS) has been widely used in biomedical materials, agricultural films, packing materials, and foaming products. However, like other aliphatic polyesters, PBS is highly combustible, which limits its application in automotive components, electronics, or the electrical industry. It is therefore necessary to provide fire resistance to PBS materials.[1–4]

To improve the flame retardancy of PBS, some flame retardants were added to PBS via melt blending. Kuan et al. prepared PBS/ammonium polyphosphate (APP) composites with improved flame retardancy and antidripping properties via a unique water-cross-linking technique. However, some of the mechanical properties of PBS decreased.[5] Chen et al. also prepared intumescent flame retardant (IFR) PBS using fumed silica as a synergistic agent. It was revealed that the lowest total loading of flame retardant could be reduced to 17% with the synergism of fumed silica for the goal of vertical flammability (UL-94) V-0 rate.[6]

Layered double hydroxides (LDHs) are a kind of layered material that can be used as a synergistic agent. Based on special structures and thermal stabilizing mechanisms, MgAlZnFe-CO_3 LDHs were prepared by the constant pH coprecipitation method in this study. Meanwhile, it is well-known that IFR are widely used as halogen-free additives owing to their advantages of little smoke and low toxicity.[7] As far as we know, little work has been reported regarding the combination of MgAlZnFe-CO_3 LDHs with IFR systems. In this work, novel IFR-PBS composites with significant flame retardancy and antidripping properties were prepared by melt blending PBS with IFR [consisting of APP and melamine (MA)], containing MgAlZnFe-CO_3 LDHs as a synergistic agent. The flame retardancies of the novel IFR-PBS composites were evaluated by limiting oxygen index (LOI) ,vertical flammability (UL-94) tests, and Cone calorimeter tests (CCT). The thermal properties, dynamic combustion behaviors, and residual char of the IFR-PBS composites were also evaluated.

EXPERIMENTAL

Materials

All of the chemical reagents used in this study were of A.R. grade (analytical reagent grade). PBS (M_W = 190 kDa, relative

Table I. The Composition and Naming of MgAlZnFe-CO_3 LDHs

Sample	$MgCl_2{\cdot}6H_2O$ (g)	$ZnCl_2$ (g)	$AlCl_3{\cdot}6H_2O$ (g)	$FeCl_3{\cdot}6H_2O$ (g)	NaOH (g)	Na_2CO_3 (g)
1#	18.270	4.080	7.245	2.705	10.240	8.480
2#	20.300	3.400	2.415	8.115	10.240	8.480
3#	20.300	3.400	6.762	3.787	10.240	8.480

Table II. The Composition and Naming of IFR-PBS Composites

Sample	PBS loading (%)	IFR loading (%)	LDHs loading (%)	APP : MA (ratio of mass)
PBS	100	0	0	
PI	80	20	0	5 : 1
PIF1	80	19	1	5 : 1
PIF3	80	17	3	5 : 1
PIF5	80	15	5	5 : 1
PIF7	80	13	7	5 : 1

density at 25°C of 1.26 g/cm^3, melt flow index at 190°C/2.16 kg of 11 g/10 min, hydroxyl end-capped) was purchased from Anqing Hexing Chemicals (Anhui, China). APP powder (soluble fraction in water <0.2 g/100 mL at 25°C, polymerization degree >1000) was obtained from Kunshan Golden Yikun Fire Retardant Materials (Jiangsu, China). MA was provided by the National Medicine Group Chemical Agent (Shanghai, China). All chemicals were dried in an oven overnight at 70°C before being used.

Preparation of MgAlZnFe-CO_3 LDHs

MgAlZnFe-CO_3 LDHs was prepared by the constant pH coprecipitation method. The composition and naming of MgAlZnFe-CO_3 LDHs are listed in Table I. At first, $MgCl_2{\cdot}6H_2O$, $AlCl_3{\cdot}6H_2O$, $ZnCl_2$ and $FeCl_3{\cdot}6H_2O$ were dissolved in deionized water to obtain a metal salt solution. And NaOH and Na_2CO_3 were dissolved in the same volume deionized water to obtain an alkaline solution. Subsequently, both solutions were added simultaneously to homemade reaction vessels, maintaining a constant pH of 10 until the end of the reaction. Then the resulting slurry was kept under vigorous stirring at 90°C for 8 h. After that, it was washed repeatedly with deionized water until the pH of the filtrate was around 7 and dried at 70°C for 24 h. Finally, the precipitate was grinded into a fine powder after drying.

Preparation of IFR-PBS Composites

The composition and naming of IFR-PBS composites are listed in Table II. During the preparation of the IFR-PBS composites, MgAlZnFe-CO_3 LDHs, and IFR (consisting of APP and MA) were melt blended with PBS at 115°C using a twin-screw extruder (CTE-35, Coperion, China) after the components were physically premixed in a high-speed mixer (SHR-10A, Gelan, China) for 15 min at room temperature. Then, the extruded strands were cooled in a cold water bath, pulled, pelletized into granules, and dried at 70°C for 8 h before injection molding. By using a screw injection-molding machine (HTF90WE, HAITIAN, China), the IFR-PBS composite pellets were injection molded into ASTM standard specimens for mechanical and flame retarded measurements at 115°C with an injection pressure of 30 MPa. All of the specimens were conditioned at 23°C for 48 h before testing.

Methods of Characterization

X-ray Diffractometer (XRD). XRD patterns were recorded on a diffractometer (40 kV, 100 mA; *D*/max-2500, Rigaku, Japan), using Cu Kα radiation at a scanning rate of $2\theta = 5°$/min (from 10° to 80°).

Inductively Coupled Plasma-Atomic Emission Spectrometer (ICP-ES). Element analysis (Mg, Al, Zn, and Fe content) were determined by ICP-ES (PS-6, Baird) after dissolution of the solids by an HCl acid solution.

Fourier Transform Infrared (FTIR) Spectroscopy. FTIR spectras were measured on an FTIR Spectrometer (380, Nicolet) with wavenumbers of 400–4000 cm^{-1} using pressed KBr pellets.

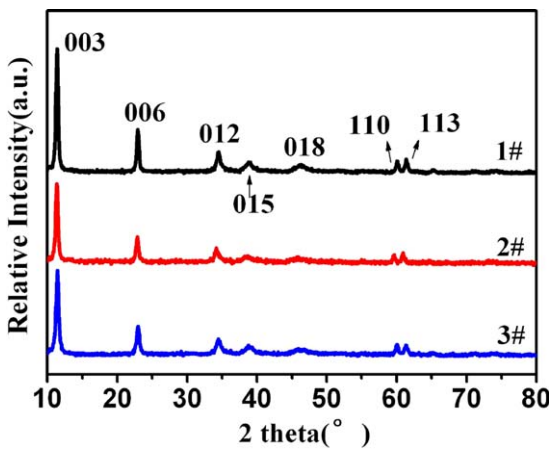

Figure 1. XRD patterns of MgAlZnFe-CO_3 LDHs prepared at different proportions. [Color figure can be viewed in the online issue, which is available at wileyonlinelibrary.com.]

Table III. Lattice Parameters of XRD Patterns for LDHs at Different Proportions

Sample	M^{2+}/M^{3+}	Fe^{3+}/M^{3+}	$d_{(003)}$ (nm)	$d_{(006)}$ (nm)	a^a (nm)	c^b (nm)
1#	3.0000	0.2500	0.7822	0.3951	0.3554	2.3878
2#	3.1250	0.7500	0.7821	0.3971	0.3526	2.4019
3#	2.9762	0.3333	0.7670	0.3888	0.3552	2.3606
MgAl-CO_3 LDHs	2.0000	0	0.7368	0.3728	0.3028	2.2100

[a] It is well-known that LDHs belongs to the hexagonal system, where the lattice parameter a ($=2d_{110}$) is a function of the average radii of the metal cations in the layers and reflects the density of metal ions stacking in the (003) crystal plane.
[b] The lattice parameter c ($=d_{003}+2d_{006}+3d_{009}$) is a measure of the thickness of the crystal cell.

Thermogravimetric Analysis (TGA). TGA was conducted from 30 to 600°C using a thermoanalyzer instrument (Q500, TA) under a flowing nitrogen atmosphere at a scan rate of 10°C/min. T_{max} (T_{max1} or T_{max2}) and T_0, defined as the temperature at the (first or second) maximum weight loss rate and that corresponding to a 5% weight loss, respectively, were measured. The calculated TG curves of PIF1and PIF3 were computed by linear combination of the TG curves of neat PBS, IFR, and MgAlZnFe-CO_3 LDHs. The formula was as follows,

$$W_{cal}(T)_{composites} = x \times W_{exp}(T)_{PBS} + y \times W_{exp}(T)_{IFR} + z \times W_{exp}(T)_{LDHs}; x+y+z = 1$$

where $W_{exp}(T)_{PBS}$ was the value of the weight given by the experimental TGA curve of pure PBS, $W_{exp}(T)_{IFR}$ was the value of the weight given by the experimental TGA curve of IFR, $W_{exp}(T)_{LDHs}$ was the value of the weight given by the experimental TGA curve of MgAlZnFe-CO_3 LDHs, and x, y, and z were the weight percents of the PBS, IFR, and MgAlZnFe-CO_3 LDHs in the composite, respectively.

Scanning Electron Microscopy (SEM). The surface morphologies of synthesized MgAlZnFe-CO_3 LDHs, IFR-PBS composites and IFR-PBS composites after combustion were observed using SEM (6380LV, JEOL, Japan) at an accelerating voltage of 10 kV (for the LDHs) and 25 kV (for the IFR-PBS composites). The fracture surface was coated with a thin layer of gold before measurement.

Differential Scanning Calorimetry (DSC). DSC analysis was performed on a differential scanning calorimeter (Q20, TA). The samples were heated to 140°C at 100°C/min and kept at this temperature for 5 min before cooling down to assure that the materials melted uniformly and to eliminate any thermal history. The samples were cooled down to room temperature at a cooling rate of 15°C/min. To estimate the % of crystallinity (χ), the following equation was used,

Table IV. Approximate Chemical Formulas of MgAlZnFe-CO_3 LDHs

Sample	Approximate chemical formulas
1#	$Mg_{0.59}Zn_{0.16}Al_{0.19}Fe_{0.06}(OH)_2(CO_3)_{0.12}{\cdot}0.80H_2O$
2#	$Mg_{0.62}Zn_{0.06}Al_{0.06}Fe_{0.18}(OH)_2(CO_3)_{0.12}{\cdot}0.84H_2O$
3#	$Mg_{0.62}Zn_{0.14}Al_{0.17}Fe_{0.11}(OH)_2(CO_3)_{0.12}{\cdot}0.84H_2O$

$$\chi = \frac{\Delta H}{\Delta H^0 \times \varphi} \times 100\%$$

where ΔH was the enthalpy of crystallization of the sample analyzed (J/g), ΔH^0 was a reference value that represented the enthalpy of crystallization for a 100% crystalline polymer, and φ was the mass percentage of PBS. For PBS, ΔH^0 was 210 J/g.[8] In addition, T_p defined as the temperature at exothermic crystallization peak.

Mechanical Properties. The mechanical properties were measured on a universal testing machine (CMT4104, Shenzhen New Think Material Detection, China). Tensile test procedures followed the ASTM D 638-82 method. Flexural tests followed the ASTM D 790 method.

Limiting Oxygen Index. The LOI test was carried out with an oxygen index meter (JF-5, Jiangning Analysis Instrument Company, China). The test was measured according to ASTM D2863.

UL-94 Burning Tests (UL 94). The UL-94 burning test was measured with an instrument (SH5304, Guangzhou Sunho Electronic Equipment, China). The test was performed according to the vertical burning test standard, suspended vertically above a cotton patch. The classifications were defined according to the American National Standard UL-94.

Cone Calorimeter Tests. Dynamic combustion behaviors of the samples were characterized by CCT (Fire Testing Technology,

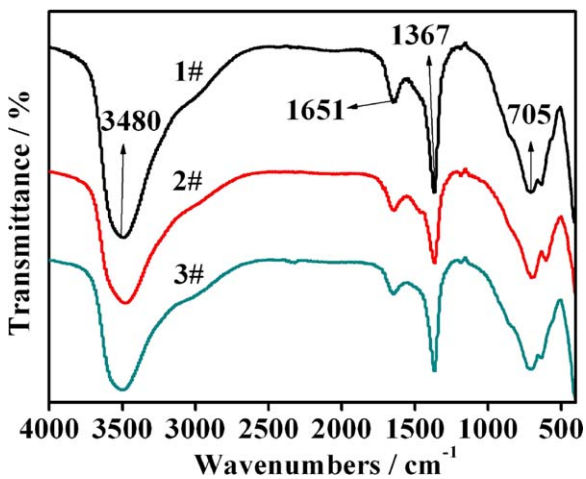

Figure 2. FTIR curves of MgAlZnFe-CO_3 LDHs prepared at different proportions. [Color figure can be viewed in the online issue, which is available at wileyonlinelibrary.com.]

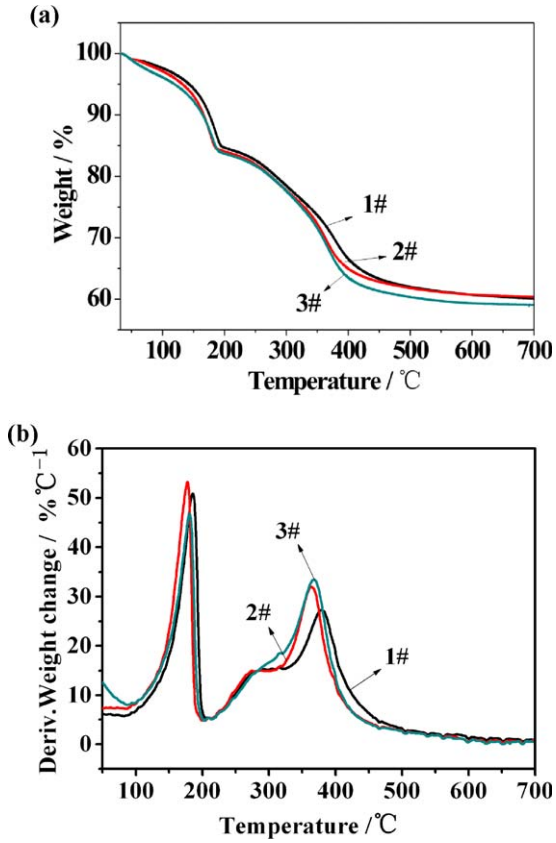

Figure 3. The (a) TG and (b) DTG graphs of MgAlZnFe-CO_3LDHs prepared at different proportions. [Color figure can be viewed in the online issue, which is available at wileyonlinelibrary.com.]

UK) according to ISO 5660. Samples were irradiated horizontally at a heat flux of 25 kW m^{-2}. All measurements were repeated three times and the results were averaged.

Laser Raman Spectroscopy (LRS). Graphite structures on the outer and inner surfaces of the char layer were characterized by LRS (LabRAM Aramis, HJY, France), using a laser transmitter at a wavelength of 633 nm from 500 to 2000 cm^{-1}.

RESULTS AND DISCUSSION

XRD and ICP-ES

The XRD patterns of MgAlZnFe-CO_3 LDHs prepared at different proportions are shown in Figure 1. The XRD patterns of MgAlZnFe-CO_3 LDHs showed almost identical characteristics (JCPDS file no. 38-0487). It can be seen in Figure 1 that the diffraction peaks were sharp and symmetrical, and the baseline was low and stable, indicating relatively well-formed crystalline

Table V. Thermal Properties of MgAlZnFe-CO_3 LDHs

Sample	T_0 (°C)	T_{max1} (°C)	T_{max2} (°C)	Char residue at 600 (°C/%)
1#	143	186	382	60.09
2#	132	180	370	60.36
3#	120	183	373	59.07

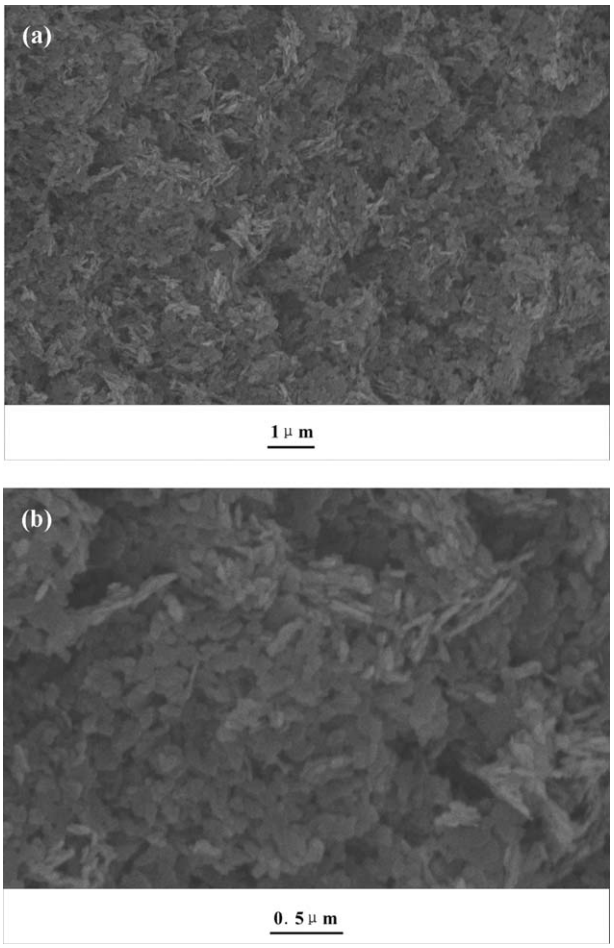

Figure 4. SEM photographs of MgAlZnFe-CO_3 LDHs. Scale: (a) 10,000× and (b) 30,000×.

layered structures. The characteristic reflections (003), (006), and (110) were easily recognized in all patterns.[9,10]

According to crystal indices and spacing, lattice parameters from the different proportions are given in Table III. Compared with MgAl-CO_3 LDHs, lattice parameters *a* and *c* of MgAlZnFe-CO_3 LDHs could be increased by the addition of Fe^{3+} and

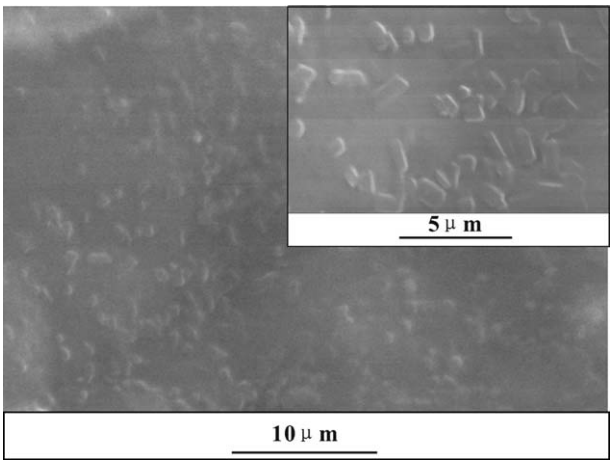

Figure 5. SEM photographs of PIF1. Scale: (a) 3000× and (b) 9000×.

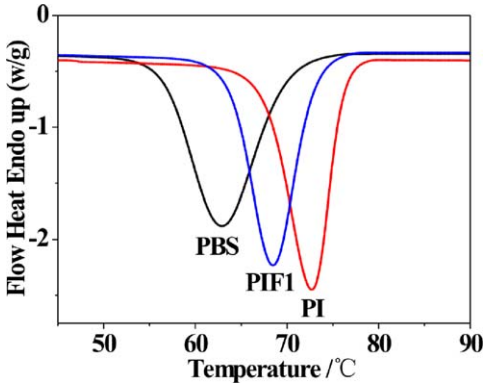

Figure 6. The DSC exothermic curves of IFR-PBS composites and pure PBS. [Color figure can be viewed in the online issue, which is available at wileyonlinelibrary.com.]

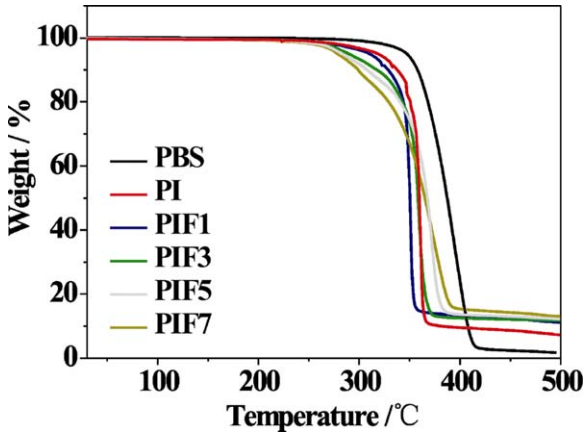

Figure 7. The TG patterns of IFR-PBS composites and pure PBS. [Color figure can be viewed in the online issue, which is available at wileyonlinelibrary.com.]

Table VI. The Crystallization Performance Parameters of IFR-PBS Composites

Sample	T_p (°C)	$\triangle H_c$ (Jg^{-1})	X_c (%)	$t_{1/2}$ (min)
PBS	62.8	54.3	25.9	0.95
PI	72.7	47.5	28.3	0.45
PIF1	68.4	47.2	28.1	0.55

Zn^{2+} (the ionic radii of Mg^{2+}, Zn^{2+}, Al^{3+}, and Fe^{3+} are 0.072, 0.074, 0.054, and 0.064 nm, respectively). The increase of lattice parameters suggests a distortion of the LDHs network induced in the process of Mg^{2+} and Al^{3+} being partially substituted for by Zn^{2+} and Fe^{3+}, respectively, resulting in some change in the octahedron structure, which centers on metal ions. This increased the layer plate thickness (lattice parameter *c*) and the average distance between the metal ions (lattice parameter *a*).[11,12] For example, the lattice parameters of 1# MgAlZnFe-CO_3 LDHs increased by 17% in lattice parameter *a*, and 8% in lattice parameter *c*.

The approximate chemical formulas, calculated from the metal ion content and the water content determined from the weight loss by heating at 250°C, are given in Table IV. The hydroxide content was calculated on the basis of electrical neutrality and mass conservation.

Fourier Transform Infrared

In Figure 2, the FTIR curves were very similar for MgAlZnFe-CO_3 LDHs at different proportions. For 1# MgAlZnFe-CO_3 LDHs, the broad peak around 3480 cm^{-1} can be ascribed to the stretching of the O—H groups attached to the metal ions. The bending vibration of the interlayer water was found to be 1651 cm^{-1}. The presence of CO_3^{2-} was confirmed by the peaks near 1367 and 705 cm^{-1}, which corresponded to antisymmetric stretching vibrations and bending vibrations in the carbonyl group. Compared with the stretching vibrations of CO_3^{2-} in $CaCO_3$ (at 1430 cm^{-1}), the peak position of CO_3^{2-} in MgAlZnFe-CO_3 LDHs shifted to lower wave numbers. The results indicated that CO_3^{2-} were not really acting freely in MgAlZnFe-CO_3 LDHs. The bands recorded below 700 cm^{-1}, especially the sharp and strong characteristic band around 420 cm^{-1}, appeared due to the vibration of metal-oxygen bonds in the brucite-like lattice.[13]

Thermogravimetric Analysis

The TG and DTG curves of MgAlZnFe-CO_3 LDHs are shown in Figure 3, and the related data are listed in Table V. All MgAlZnFe-CO_3 LDHs appeared at two weight loss intervals. The first mass loss, from room temperature to ~200°C, was mainly assigned to the removal of the interlayer and weakly adsorbed water; the second gradual mass loss, which occurred in the temperature range of 200–550°C, was mainly ascribed to the dehydroxylation of the lattice and the evolution of CO_2, which was formed by the thermal decomposition of the interlayer CO_3^{2-} anions. The laminate of MgAlZnFe-CO_3 LDHs collapsed when the temperature exceeded 600°C, which

Table VII. Mechanical Properties of IFR-PBS Composites and Pure PBS

Sample	Tensile Strength (MPa)	Elongation at break (%)	Flexural Strength (MPa)
PBS	27.3 ± 0.5	40.3 ± 0.8	18.2 ± 0.7
PI	21.5 ± 0.8	35.4 ± 1.2	19.6 ± 0.9
PIF1	23.5 ± 0.2	37.4 ± 1.1	21.4 ± 0.6
PIF3	24.0 ± 0.5	31.3 ± 1.6	21.7 ± 0.8
PIF5	25.1 ± 0.8	25.3 ± 0.4	22.9 ± 0.5
PIF7	25.3 ± 0.4	23.1 ± 1.0	22.0 ± 0.6

Table VIII. Thermal Properties of IFR-PBS Composites

Sample	T_0 (°C)	T_{max} (°C)	Char residue at 600 (°C/%)
PBS	348	394	0
PI	312	339	5.86
PIF1	310	346	9.09
PIF3	290	357	11.28
PIF5	282	380	12.25
PIF7	279	376	12.42

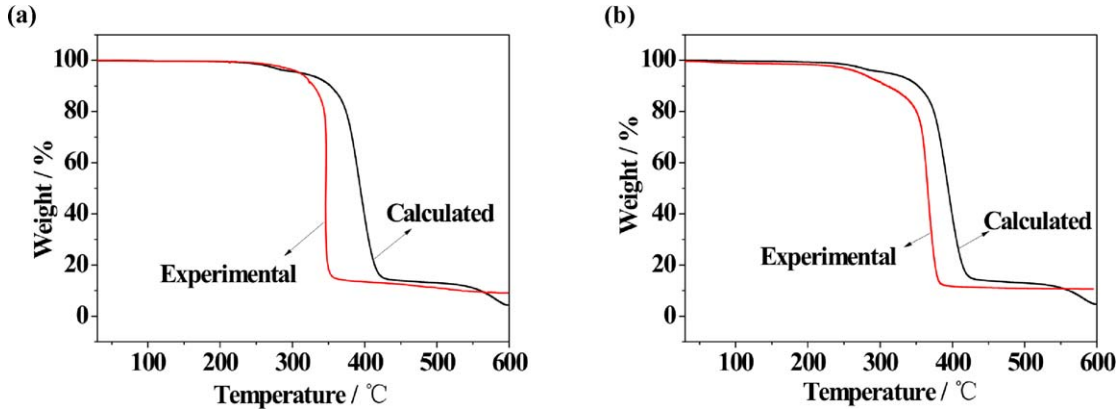

Figure 8. Weight differences between experimental and theoretical TG curves for (a) PIF1 and (b) PIF3. [Color figure can be viewed in the online issue, which is available at wileyonlinelibrary.com.]

transformed it into a composite metal oxide. DTG also profiled the first two events, which were accompanied by two endothermic peaks.[14] TG tests showed that all MgAlZnFe-CO_3 LDHs represented the peculiar weightlessness characteristics of LDHs.

All samples of MgAlZnFe-CO_3 LDHs had similar char residues at 600°C. However, the T_0 and T_{max} of the 1# MgAlZnFe-CO_3 LDHs both increased in comparison to the others. This indicated that 1# MgAlZnFe-CO_3 LDHs had better thermal stability in processed PBS.

Scanning Electron Microscopy

Typical SEM photographs of MgAlZnFe-CO_3 LDHs are shown in Figure 4. Figure 4 indicated lamellar particles that looked like rounded hexagonal shapes, which is typical of hydrotalcite-like materials.[14] Obviously some fragments occurred when Fe^{3+} was introduced into the layers. However, the expected hexagonal plate-like nature of the crystallites was clearly apparent in each case. The average diameter of the platelets was <200 nm.[15]

From Figure 5, it can be seen that MgAlZnFe-CO_3 LDHs dispersed uniformly in the PBS matrix (PIF1), as a result of the sufficient shear force imposed during the melt compounding process. A small amount of aggregates, which exceeded 500 nm in diameter, were observed as a result of the interactions between the MgAlZnFe-CO_3 LDHs.[16]

Differential Scanning Calorimetry

Nonisothermal crystallization experiments were conducted with DSC cooling scans of the pure PBS and IFR-PBS composites at a cooling rate of 15°C/min, and the results are shown in Figure 6 with related crystallization parameters listed in Table VI. Only one exothermic peak temperature was observed for each curve between 40 and 90°C. The crystallization parameters illustrated in Table VI indicated that the addition of IFR increased T_p (increase from 62.8 to 72.7°C) and the crystallization rate. Furthermore, the degree of crystallinity (increase from 25.9 to 28.3%) increased with the addition of IFR. It was seen that IFR may act as a nucleating agent in the crystallization process of PBS.

The crystallization behavior of PIF1 indicated that the addition of MgAlZnFe-CO_3 LDHs reduced the crystallization temperature and crystallization enthalpy of IFR-PBS composites. However, the half-peak width of IFR-PBS composites did not change, thus indicating that the LDHs and PBS matrix have strong hydrogen bond interactions.[17] Meanwhile, the crosslinking reaction between PBS, IFR, and MgAlZnFe-CO_3 LDHs eliminated the heat history, resulting in an increase of system viscosity. The addition of MgAlZnFe-CO_3 LDHs also imposed restrictions on the molecular chain segment movement of PBS, and restricted crystal nucleation and crystal growth.[18,19] Furthermore, the slight reduction in the degree of crystallinity suggested the refinement of crystal grains.[20]

Mechanical Properties

The effect of MgAlZnFe-CO_3 LDH content on the tensile strength and flexural strength of IFR-PBS composites is shown in Table VII. Table VII showed that adding MgAlZnFe-CO_3 LDHs increased the tensile strength of IFR-PBS composites from 21.5 to 25.3 MPa (an 18% increase) as MgAlZnFe-CO_3 LDH content increased from 0 to 7%. According to the analysis of the crystallization behavior, IFR-PBS composites treated with MgAlZnFe-CO_3 LDHs exhibited better tensile strength than untreated ones due to superior interfacial bonding. Moreover, IFR-PBS composites with MgAlZnFe-CO_3 LDHs exhibited a smaller elongation-at-break as compared with virgin ones, as a result of rigid inorganic particles of negative effect on toughness.[21]

Table IX. LOI and UL-94 Results of IFR-PBS Composites and Pure PBS

Sample	LOI (%)	UL-94 rate	Dripping	Ignite the absorbent cotton
PBS	24	NR	Yes	Yes
PI	30	V-1[a]	No/Yes[b]	No
PIF1	35	V-0[a]	No	No
PIF3	33	V-0	No/Yes[b]	No
PIF5	25	V-2[a]	Yes	Yes
PIF7	24	V-2	Yes	Yes

[a] V-0 rate is after flame within 10 s, no dripping or cotton ignition. V-1 rate is after flame within 30 s, no dripping or cotton ignition. V-1 rate is afterflame within 30 s, cotton ignited by flaming particles or drops.
[b] No/Yes corresponds to the first/second flame application.

Table X. Cone Calorimeter Results for IFR-PBS Composites and Pure PBS

Sample	TTI (s)	Peak-HRR (kW m^{-2})	Peak-SPR (m^2 s^{-1})	Peak-MLR (g s^{-1})	THR MJ (m^{-2})	TSP (m^2 m^{-2})	CO Yield (kg kg^{-1})	FPI (s m^2 kW^{-1})
PBS	200	368	0.032	0.216	102	592	0.092	0.543
PI	124	313	0.024	0.159	80	667	3.903	0.396
PIF1	143	258	0.019	0.069	83	351	1.971	0.554
PIF3	151	250	0.022	0.066	84	526	1.681	0.604

Adding MgAlZnFe-CO_3 LDHs to IFR-PBS composites increased the flexural strength markedly. The flexural strength of IFR-PBS composites increased from 19.6 to 22.9 MPa (a 17% increase) when the MgAlZnFe-CO_3 LDH content increased from 0 to 5%. However, adding more MgAlZnFe-CO_3 LDHs to the IFR-PBS composites could reduce the flexural strength of the IFR-PBS composites as a result of the reduced plasticity of the IFR-PBS composites.

Thermogravimetric Analysis

Figure 7 shows the TG patterns of the IFR-PBS composites. The thermal degradation properties and related data are listed in Table VIII. The T_0 of the IFR-PBS composites decreased by 2 to 33°C with the addition of MgAlZnFe-CO_3 LDHs, which may be due to the catalytic effect of MgAlZnFe-CO_3 LDHs on the decomposition of IFR (APP and MA). The char residue increased from 5.86 (PI) to 9.09% (PIF1) (a 55% increase) at 600°C as the MgAlZnFe-CO_3 LDH content increased from 0 to 1%. This indicated that the synergistic effect between IFR and MgAlZnFe-CO_3 LDHs could catalyze the char formation of PBS at high temperatures. Moreover, the maximum degradation temperature (T_{max}) of the IFR-PBS composites increased gradually in comparison with that of PI. Regarding the analyses above, a conclusion could be drawn that the addition of MgAlZnFe-CO_3 LDHs improved the char residue and thermal stability properties.[22]

To further investigate the MgAlZnFe-CO_3 LDHs-IFR synergism, the weight differences between the experimental and theoretical

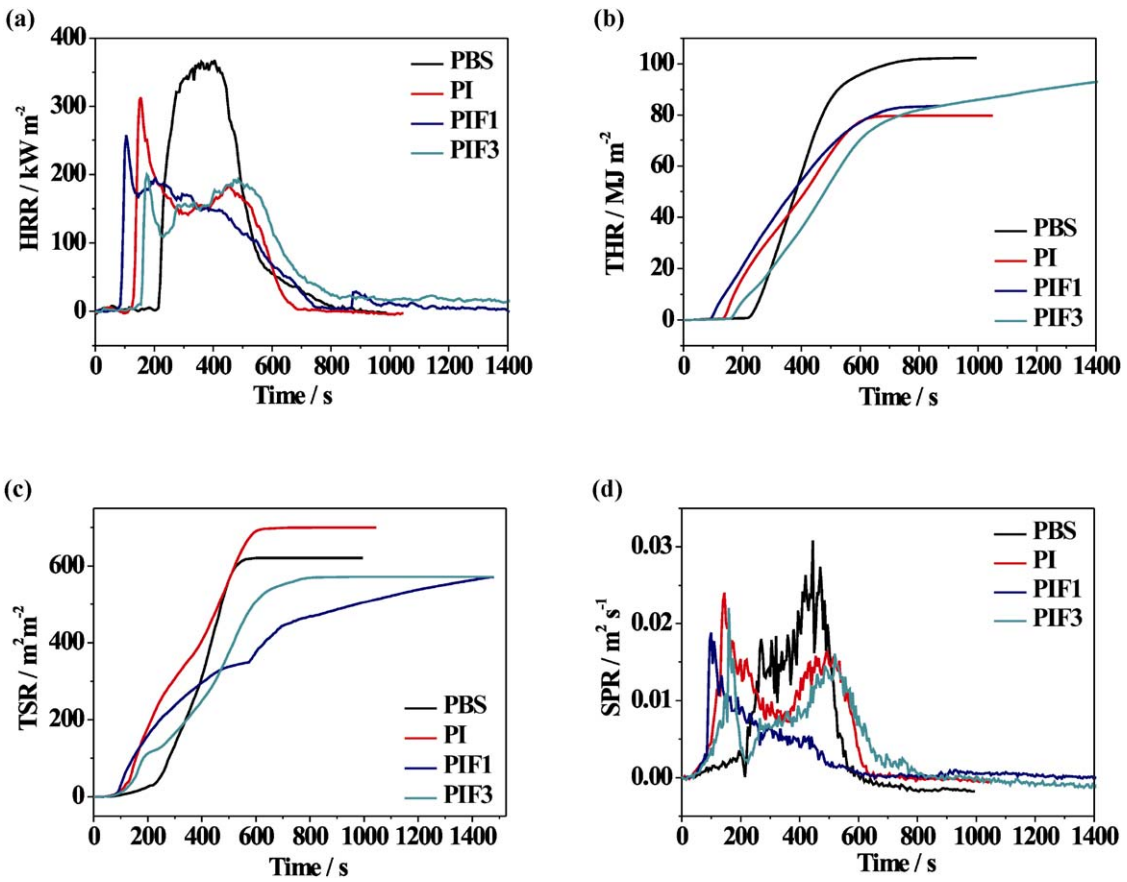

Figure 9. (a) Heat release rate and (b) THR curves for IFR-PBS composites and pure PBS. [Color figure can be viewed in the online issue, which is available at wileyonlinelibrary.com.]

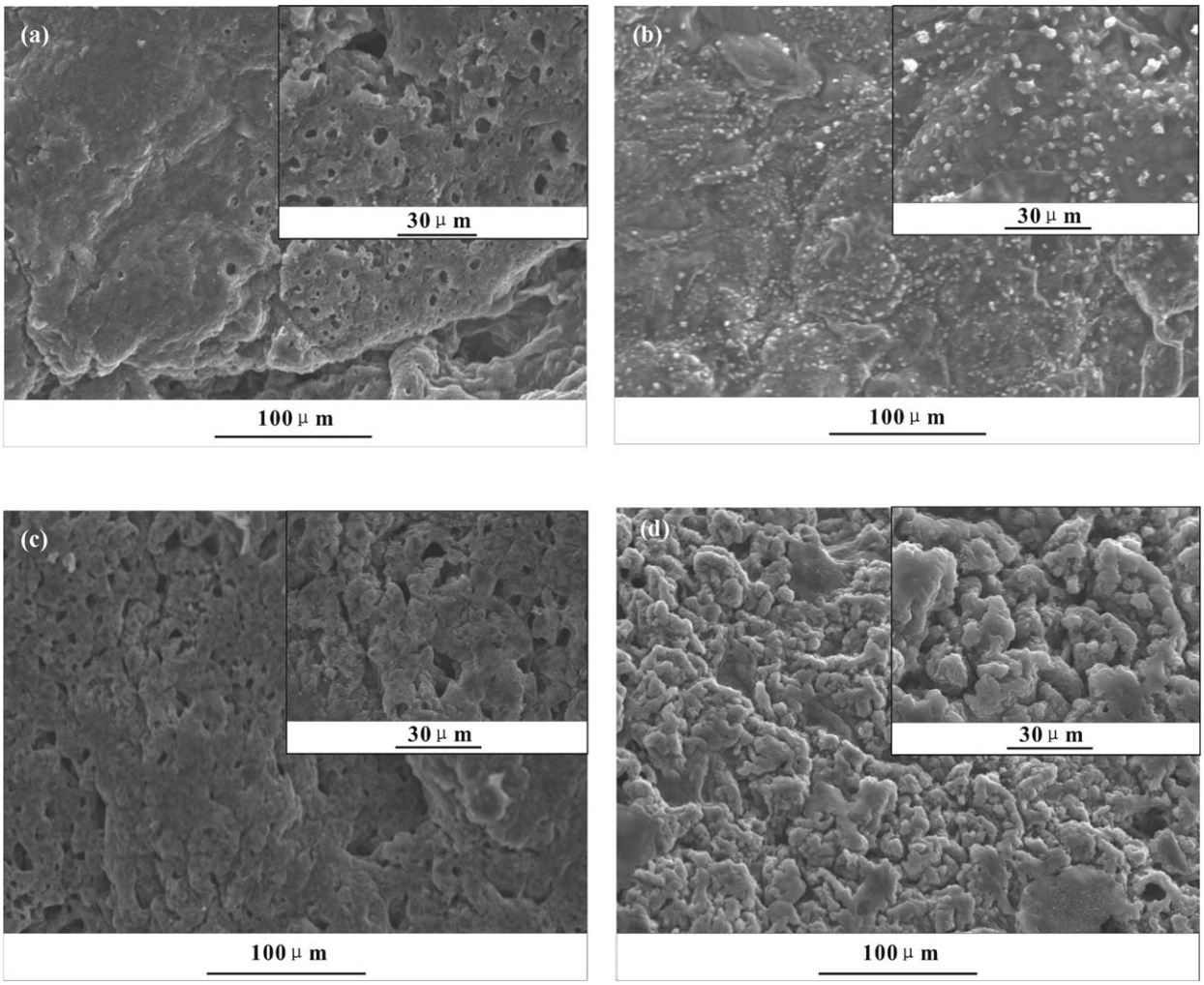

Figure 10. SEM images of IFR-PBS composites after combustion: (a) PI, (b) PIF1, (c) PIF3, and (d) PIF5.

TG curves for PIF1 and PIF3 are presented in Figure 8. As can be seen, T_0 in the experimental curves was lower than that in the calculated ones, suggesting catalysis of MgAlZnFe-CO_3 LDHs impact on the decomposition. However, in the temperature range of 300 to 350°C, the experimental curves showed faster thermal degradation than the calculated ones. It was also observed that MgAlZnFe-CO_3 LDHs changed the degradation process of IFR and PBS, and that MgAlZnFe-CO_3 LDHs promoted char formation, which is beneficial to improving the thermal stability and flame retardancy performance of the IFR-PBS composites.

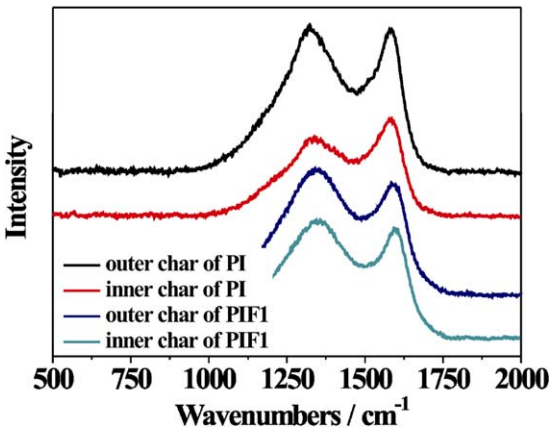

Figure 11. Raman spectra of the outer and inner char residue for PI and PIF1 after combustion. [Color figure can be viewed in the online issue, which is available at wileyonlinelibrary.com.]

Flammability

From Table IX, it can be seen that the LOI value of PIF1 obtained a maximum of 35, which was 11 units higher than

Table XI. Results of Raman Analysis of Outer and Inner Char for PI and PIF1

Sample	Char layer	$A_{D\ band}$[b]	$A_{G\ band}$[b]	$R = A_D/A_G$
PI	outer	458,000	151,000	3.03
	inner	263,000	99,780	2.64
PIF1	outer	443,300	153,600	2.89
	inner	430,700	161,200	2.67

[a] The area of the D or G band.

that of pure PBS. In addition, a UL-94 V-0 rate was achieved. The flame resistance of IFR-PBS composites overall declined when the MgAlZnFe-CO_3 LDH content exceeded 3%. The reason for this may lie in the relatively large amounts of inorganic particles (MgAlZnFe-CO_3 LDHs) which embrittled the expansion carbon layer.[23,24]

CCT provided abundant information on the combustion properties of the investigated materials, including the time-to-ignition (TTI), the heat release rate (HRR), the total heat release (THR), the smoke production rate (SPR), the total smoke produced (TSP), and CO yield during combustion. These data and some derived parameters such as the fire performance index (FPI, defined as the ratio of TTI and Peak-HRR. The larger value means the higher security.) are presented in Table X. Figure 9 illustrates the HRR, THR, SPR, and TSP as a function of time for formulations filled with MgAlZnFe-CO_3 LDHs (a–d).

After ignition, PBS showed one single well-defined peak in the HRR curve with a peak value of 368 kW m^{-2}. The presence of IFR in the PBS decreased the Peak-HRR value of PBS by 15% and decreased the time-to-Peak-HRR. There was also a shoulder peak in the HRR curves. In the formulation containing 1% MgAlZnFe-CO_3 LDHs (PIF1), there was a significant change in Peak-HRR compared to PI. In addition, adding more MgAlZnFe-CO_3 LDHs further decreased the Peak-HRR. Combining IFR and MgAlZnFe-CO_3 LDHs in PBS resulted in a significant decrease in Peak-HRR and Peak-SPR values. For PIF1, the Peak-HRR and THR were significantly reduced, by 30 and 36%, respectively, compared with those of pure PBS.[25]

Analysis of Intumescent Char

To investigate the relationship between the microstructure of intumescent char and the flame retardancy of IFR-PBS composites, the intumescent char residue (heated in a muffle furnace for 10 min at 600°C) of PI, PIF1, PIF3, and PIF5 were imaged by SEM and magnified 350 and 1200 times, as shown in Figure 10. As shown in Figure 10(a,c,d), it could be observed that there were some cracks and spots on the outer char of PI. Therefore, PI could not provide a good flame shield for PBS. In contrast, as shown in Figure 10(b), the outer char of PIF1 was more compact than that of PI, and had lot of bubbles. The compact intumescent charred layer slowed the heat and mass transfer between gas and condensed phases, and prevented the underlying polymeric substrate from further attack by heat flux in a flame.

Raman spectra are usually used to characterize the graphitic structure of materials, and to evaluate the order degree of carbon materials in terms of two characteristic bands: the D band (1340 cm^{-1}, associated with vibration of carbon atoms with dangling bonds in the plane terminations of disordered graphite or glass carbons, representing the unorganized carbon structure) and the G band (1580 cm^{-1}, corresponding to an E2g mode of hexagonal graphite and related to the vibration of sp2-bond carbon atoms in graphite layers, showing the graphitic structure).[26] Figure 11 presents the Raman spectra of the outer and inner char residue for PI and PIF1 after combustion. Each spectrum was subjected to peak fitting using the curve fitting software Origin 8.5/Peak Fitting Module to resolve the curve into two Gaussian bands. It was noted that all of them displayed two visible bands, and that these observations provided positive evidence for the formation of polyaromatic species or graphitic structures.[27] Tuinstra and Koenig found that the relative intensity ratio R of the D peak to the G peak was inversely proportional to an in-plane microcrystalline size and/or an in-plane phonon correlation length obtained from Raman spectroscopy.[28] Therefore, the T-K relation is a good indicator of the graphitization degree of carbon materials, where the higher the value of R, the lower the graphitization degree of the char. Table XI gives the results of Raman analysis of the outer and inner char for PI and PIF1. The R of outer chars of PI and PIF1 decreased from 3.03 to 2.89, which indicated that a more graphitic structure formed. However, as to the inner char, the R changed little when MgAlZnFe-CO_3 LDHs was incorporated, thus indicating that a more amorphous carbon structure formed. It can be concluded that upon ignition, MgAlZnFe-CO_3 LDHs can turn amorphous char into a graphitic structure on the outer surface, where the strength of the outer char is enhanced and becomes more compact.

CONCLUSIONS

In this article, novel IFR-PBS composites were prepared. With 1% MgAlZnFe-CO_3 LDHs (the total content of flame retardant was 20%), IFR-PBS composites achieved a LOI value of 35 and a UL-94 V-0 rate. Analysis of the thermal properties (TG) and dynamic combustion behaviors (CCT) indicated that the presence of MgAlZnFe-CO_3 LDHs could change the decomposition behavior of IFR-PBS composites, and enhance the fire retardant performance, consequently resulting in a large reduction in the peak heat release rate (PEAK-HRR) and SPR of IFR-PBS composites. SEM and LRS measurements illustrated that MgAlZnFe-CO_3 LDHs promoted the formation of compact char structures. A proper formulation between IFR (consisting of APP and MA) and MgAlZnFe-CO_3 LDHs in IFR-PBS composites showed optimal synergistic effects. Moreover, tensile strength and flexural strength were improved by the presence of MgAlZnFe-CO_3 LDHs.

ACKNOWLEDGMENTS

This study was supported by the National Natural Science Foundation of China (No. 11372108), the New Century Excellent Talent of the Ministry of Education of China (No. NCET-10-0161), the Hunan Science and Technology Project (No. 2010FJ4127), and the University Innovation Platform Development Fund of Hunan Province (No. 13K098).

REFERENCES

1. Ray, S. S.; Okamoto, K.; Okamoto, M. *Macromolecules* **2003**, *36*, 2355.
2. Papageorgiou, G. Z.; Bikiaris, D. N. *Polymer* **2005**, *46*, 12081.
3. Tachibana, Y.; Masuda, T.; Funabashi, M.; Kunioka, M. *Biomacromolecules* **2010**, *11*, 2760.

4. Wu, K.; Hu, Y.; Song, L.; Lu, H. D.; Wang, Z. Z. *Ind. Eng. Chem. Res.* **2009**, *48*, 3150.
5. Kuan, C. F.; Kuan, H. C.; Ma, C. C. M.; Chen, C. H. *J. Appl. Polym. Sci.* **2006**, *102*, 2935.
6. Chen, Y. J.; Zhan, J.; Zhang, P.; Nie, S. B.; Lu, H. D.; Song, L.; Hu, Y. *Ind. Eng. Chem. Res.* **2010**, *49*, 8200.
7. Wu, K.; Shen, M. M.; Hu, Y. *Polym. Plast. Technol. Eng.* **2010**, *49*, 1527.
8. Papageorgiou, G. Z.; Bikiaris, D. N. *Polymer* **2005**, *46*, 12081.
9. Zhang, L. H.; Li, F.; Evans, D. G.; Duan, X. *Ind. Eng. Chem. Res.* **2010**, *49*, 5959.
10. Valente, J. S.; Sanchez–Cantu, M.; Lima, E.; Figueras, F. *Chem. Mater.* **2009**, *21*, 5809.
11. Benselka–Hadj Abdelkader, N.; Bentouami, A.; Derriche, Z.; Bettahar, N.; Menorval, L. C. *Chem. Eng. J.* **2011**, *169*, 231.
12. Chen, Y. F.; Li F.; Yu, G. S.; Yang, X. J. *Spectrochim. Acta Part A* **2012**, *86*, 625.
13. Iwasaki, T.; Shimizu, K.; Nakamura, H.; Watano, S. *Mater. Lett.* **2012**, *68*, 406.
14. Pfeiffer, H.; Lima, E; Lara, V.; Valente, J. S. *Langmuir* **2010**, *26*, 4074.
15. Delorme, F.; Seron, A.; Giovannelli, F.; Beny, C.; Jean–Prost, V.; Martineau, D. *Solid State Ionics* **2011**, *187*, 93.
16. Wang, X.; Hu, Y.; Song L.; Yang, H. Y.; Yu, B.; Kandola, B.; Deli, D. *Thermochim. Acta* **2012**, *543*, 156.
17. Bhattacharyya, A. R.; Sreekumar, T. V.; Liu, T.; Kumar, S.; Ericson, L. M.; Hauge, R. H.; Smalley, R. E. *Polymer* **2003**, *44*, 2373.
18. He, Q.; Yuan, T.; Zhu, J.; Luo, Z.; Haldolaarachchige, N.; Sun, L.; Khasanov A.; Li, Y.; Young D.; Wei S.; Guo, Z. *Polymer* **2005**, *53*, 3642.
19. Zhu, J.; He, Q.; Luo, Z.; Khasanov, A.; Li, Y.; Sun, L.; Wang, Q.; Wei, S.; Guo, Z. *J. Mater. Chem.* **2012**, *22*, 15928.
20. Papageorgiou, G. Z.; Achilias, D. S.; Bikiaris, D. N. *Macromol. Chem. Phys.* **2007**, *208*, 1250.
21. Pramoda, K. P.; Linh, N. T. T.; Zhang, C.; Liu, T. X. *J. Appl. Polym. Sci.* **2009**, *111*, 2938.
22. Wang, X.; Song L.; Yang, H. Y.; Lu, H. D.; Hu, Y. *Ind. Eng. Chem. Res.* **2011**, *50*, 5376.
23. Du, B. X.; Ma, H. Y.; Fang, Z. P. *Polym. Adv. Technol.* **2011**, *22*, 1139.
24. Wang, L.; Hu, Y.; Song, L.; Yuen, R. K. K. *Ind. Eng. Chem. Res.* **2012**, *51*, 15082.
25. Tang, T.; Chen, X. C.; Meng X. Y.; Chen, H.; Ding, Y. P. *Angew. Chem. Int. Ed. Engl.* **2005**, *117*, 1541.
26. Feng, C. M.; Zhang, Y.; Liu, S. W.; Chi, Z. G.; Xu, J. R. *Polym. Degrad. Stab.* **2012**, *97*, 707.
27. Song, P. A.; Fang, Z. P.; Tong, L. F.; Jin, Y. M.; Lu, F. Z. *J. Anal. Appl. Pyrolysis.* **2008**, *82*, 286.
28. Tuinstra, F.; Koenig, J. L. *J. Chem. Phys.* **1970**, *4*, 492.